INVESTIGATION OF A NOVEL METASTRUCTURE WITH TRAPPED, FLUID-FILLED UNIT CELLS

Vinícius Mauro de Souza Santos, Thiago de Paula Sales and Morvan Ouisse

Abstract This work investigates a novel metamaterial concept using the Wave-based Finite Element Method. The metamaterial comprises a periodic-like structure manufactured through fused filament deposition, featuring internal cavities filled with water. Experimental characterization of the dynamics of the periodic system without internal fluid confirms good agreement with numerical predictions obtained through frequency response function measurements. Furthermore, the dynamic behavior of the two-phase periodic metastructure is experimentally examined, where waves interact within the heterogeneous medium consisting of both fluid and solid phases. In this case, the resulting wave characteristics depend on the properties of both phases. It was shown that the fluid-filled metastructure exhibits vibration reduction through the whole frequency range compared to the case lacking internal fluid. Additionally, it was seen that the frequency range near the second attenuation band of the periodic metastructure without fluid can be enlarged after the fluid inclusion within the cavities of its unit cells, as a consequence of mass increase and damping effects. Consequently, this work presents a promising avenue for metastructure design, with potential applications in structural dynamics and acoustics.

Keywords metamaterial · bandgap · periodic structures · fluid-structure interaction · wave-based finite element method

T. P. Sales · V. M. S. Santos (✉)
Division of Mechanical Engineering, ITA - Aeronautics Institute of Technology
São José dos Campos, Brazil
e-mail: vinicius.santos@ga.ita.br

Morvan Ouisse
SUPMICROTECH, Université de Franche-Comté, CNRS, Institut FEMTO-ST
Besançon, France

1 Introduction

The study of periodic and quasi-periodic structures opened possibilities to explore several properties that are not naturally encountered in nature, such as waveguiding [1], bandgap formation, confinement and mode localization phenomena [2], invisibility cloaks [3], mode conversion [4], and some negative equivalent properties such as refractive index, elastic modulus, and Poisson's ratio [5]. Such structures are usually referred to as metastructures just because they can exhibit apparent properties, as listed earlier, which are not typically observed in conventional systems. Probably, in the context of structural dynamics, the most studied phenomenon related to periodic structures is what one knows as bandgaps, which comprise frequency ranges where only evanescent wavemodes are allowed to occur [6]. This phenomenon can arise from Bragg-scattering [7], periodic arrangements of resonators within a host structure [5], or specially designed unit cells incorporating inertial amplification mechanisms (IAMs) [8].

In certain scenarios, both metastructures and conventional systems can exhibit complex dynamic behavior due to multiphysics problems. These may involve fluid-structure interaction (FSI), thermoelasticity, piezoelectric materials, magnetic forces, acoustic-structure interaction (ASI), viscoelasticity, and more. In this work, particular emphasis is placed on the dynamics of systems with enclosed fluid. The coupling of fluid dynamics with structural systems has been a longstanding concern in various fields, including structural engineering, aeroelasticity, hydroelasticity, vibroacoustics, wind engineering, ocean engineering, biomechanics, offshore engineering, aerospace engineering, and civil engineering. For instance, in previous research by Jamshidiat and SenGupta [9], a method based on traditional finite element (FE) procedures was developed to predict the natural frequencies and modes of an aircraft fuselage considering the enclosed fluid medium.

Although extensive research on FSI has been conducted in the aforementioned fields, it is crucial to consider the dynamics of metamaterials interacting with acoustic fluids. One notable investigation by Spadoni et al. [10] focused on studying the dynamic behavior of closed-cell crystalline foams to explore the potential of these relatively uncharted metamaterials. The authors highlighted that the complex microstructure of closed-cell crystalline foams inherently possesses internal resonances, facilitating local resonance phenomena. Through a classical vibroacoustic model, Spadoni et al. [10] demonstrated that truncated-octahedron (or Kelvin foam), face-centered cubic rhombic dodecahedron, and Weaire-Phelan foams exhibit superanisotropic properties, capable of behaving selectively as either a fluid or a solid. These foams display pentamode characteristics and feature regimes characterized by film resonances and a high density of states. These extraordinary properties can find effective utilization in various engineering and scientific disciplines, such as aerospace engineering, civil engineering, mechanical engineering, and acoustics, particularly in the design of metamaterials for specific purposes. The study of Spadoni and collaborators [10] also revealed the existence of persistent modes in the foams, i.e., those modes that remain unaffected by the presence or absence of an entrained acoustic fluid. It was observed that the propagating shear

modes, away from film resonances, are persistent modes, suggesting the hydrostatic behavior of the fluid-filled unit cell − in this case, the fluid does not influence the volumetric deformations of the foam.

Dorodnitsyn and Damme [11] introduced and experimentally investigated a novel acoustic metamaterial incorporating an entrained fluid. The authors tackled the interaction between waves traveling through combined media, consisting of both fluid and solid components, which leads to coupled elastic waves with dynamics influenced by both phases. Notably, the acoustic metamaterial studied in [11] exhibits a negative refractive index behavior, owing to the opposite signs of the system's group and phase velocity. This research has opened up a new and straightforward pathway for designing acoustic metamaterials with exceptional properties not readily found in nature. These findings hold promise for various practical engineering applications and contribute to the vibroacoustic community.

Most of the time, analytical expressions are employed with the aim of modeling the aforementioned FSI problems. However, it is well known that these expressions are limited to approximate theories, and as a result, the established models are valid only under certain specific conditions. One cannot leave mentioning that the majority of analytical models in FSI typically represent simple systems, such as fluid-filled shells. In addition, mainly seminal works published in the fifties and sixties have been focused on wave propagation behavior in empty and fluid-filled cylindrical shells with real wavenumbers, which may not accurately reflect various practical conditions [12, 13].

In an attempt to address some of these limitations, Bao et al. [14] presented closed-form expressions and conducted a theoretical study on dispersion curves of empty and fluid-filled cylindrical shells under axially symmetric waves, relying on Bessel functions, based on expressions derived by Kumar and Stephens [15]. Parametric analyses considering the wall thickness of both empty and fluid-filled systems were performed, yielding results similar to those reported in [15]. In summary, Bao et al. [14] demonstrated that dispersion curves of such cylindrical shells can exhibit purely real, purely imaginary, and complex branches. The degree of coupling between the internal fluid and the shell was found to be strongly influenced by the shell thickness. Furthermore, it was observed that the internal fluid could considerably alter the wave propagation characteristics of the cylindrical shell. It has the ability to shift the cut-off frequencies of the wavemodes, providing a valuable mean to control the dynamic behavior of a metamaterial, which was not discussed at that time. Moreover, Bao et al. [14] emphasized that certain branches seen in the dispersion curve of the fluid-filled cylindrical shell arise exclusively due to the presence of the fluid and may be purely evanescent. This realization suggests that fluid-filled systems can be exploited for designing specially engineered structures with outstanding vibration attenuation performance for those pursuing such goals.

Fuller and Fahy [16] derived closed-form expressions to predict the characteristics of elastic and acoustic wave propagation in a cylindrical elastic shell filled with fluid. The authors showed that when two fields, such as structural and acoustic, are coupled, the resulting wave behavior becomes complex. They demonstrated that when a cylindrical shell is filled with fluid, a fluid loading term arising from the presence of the fluid acoustic field must be considered in the system's free vibration. Naturally, the magnitude of this term can vary significantly , determining the level

of coupling between the shell and the fluid. Fuller and Fahy [16] also conducted several parametric analyses considering factors such as the shell wall thickness and the density ratio between the shell material and the internal fluid that provide valuable insights into the dynamics of more complex fluid-filled systems.

As seen before, earlier studies have effectively formulated analytical expressions to comprehend wave propagation in fluid-filled elastic pipes despite their inherent simplifications. These expressions often provide a clearer and easier interpretation of wave propagation phenomena compared to numerical methods. However, as discussed previously, it is widely recognized that analytical solutions have limitations, as they are constrained to simple geometries and classical wave theories. They are also constrained to a narrow range of vibroacoustic problems due to complex interactions that may occur between the acoustic fluid and the structure. To address these limitations, Mencik and Ichchou [17] resorted to a numerical method known as the Wave-based Finite Element Method (WFEM), in which the governing elasto-acoustic equations of motion are discretized using the FEM, and the problem is formulated and solved in the space spanned by wave-modes. The authors showed two mathematical strategies for handling fluid-filled structure problems: the $(\mathbf{U},\mathbf{p})$ and $(\mathbf{U},\boldsymbol{\Psi})$ formulations. In the first approach, the equations of motion for the acoustic fluid and the structure depend on the acoustic pressures of the fluid $(\mathbf{p})$ and the structural $(\mathbf{U})$ degrees of freedom (DoFs), resulting in an asymmetrical set of equations. On the other hand, the second approach is a modified version of the $(\mathbf{U},\mathbf{p})$ formulation that introduces the acoustic velocity potential $\boldsymbol{\Psi}$ to formulate the elasto-acoustic problem symmetrically. Mencik and Ichchou [17] demonstrated the robustness of their numerical approach compared to analytical formulations, such as the one presented in [16]. It was confirmed that the simplifying assumptions used in the analytical formulation are not entirely adequate and may hinder the accurate assessment of the dynamic behavior of fluid-filled systems.

Numerical methods, including the WFEM, have strengths and weaknesses in engineering applications. Challenges can arise when applying the WFEM to composite structures and FSI problems. In such cases, a fine unit cell mesh is required to accurately capture the structural dynamics. A coarse mesh can fail to predict the eigenvalues and eigenvectors related to the wave propagation characteristics throughout the system. Droz et al. [18] addressed this issue and proposed a model reduction strategy that utilizes a reduced basis to model the structural dynamic behavior. Cut-on frequencies were identified within the analyzed frequency band, which allowed for the solution of a low-order modified eigenvalue problem for these frequencies. Eigenvectors associated with propagating waves (for which the real part of the wavenumber is much greater than its imaginary part) are chosen to form the reduced basis, using an iterative scheme to avoid redundant wave shapes, and then, a reduced eigenvalue problem, with size dependent on the number of propagating waves in the analyzed frequency range, is solved. This methodology was validated through a three-layered sandwich beam, and an elastic pipe filled with acoustic fluid in ref. [18]. Additionally, Mencik [19] also presented a valuable way to increase the computational efficiency of the WFEM, based on the Craig-Bampton (CB) model order reduction technique.

From this literature overview, which addressed various modeling strategies for tackling FSI problems, and also highlighted promising applications of FSI in the

dynamics of metamaterials, in this study one aims to propose a novel concept of metamaterial with completely closed unit cells filled with water, as depicted in Fig. 1. In this illustration, the metastructure consists of six identical unit cells, with the internal cavity represented by the blue color, indicating the confined water. Firstly, a numerical model of the system without internal fluid is developed using the WFEM. Based on the Bloch-Floquet theorem and the matrices provided by the FEM, dispersion curves for the underlying unit cell are computed. Experimental frequency response functions (FRFs) for longitudinal and bending dynamics, obtained through hammer tests, are also made available and compared with numerical predictions. Subsequently, the dynamic behavior of the proposed fluid-filled metastructure is experimentally evaluated in order to understand its dynamic characteristics.

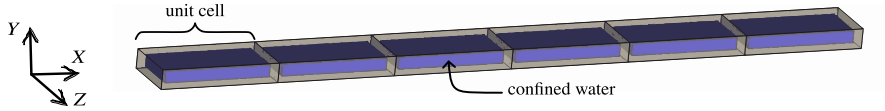

Fig. 1 A periodic metastructure filled with water fluid consisting of six identical unit cells.

Beyond this introduction, this work has been divided into five sections. First, in Section 2, we review the WFEM, which can be used to model the fluid-filled metastructure shown in Fig. 1. Dispersion curves and numerical and experimental FRFs are shown in Section 3. Discussions about the dynamics of the system with and without fluid are supplied, as well. A summary of our findings and conclusions are given in Section 4. Acknowledgments and references are provided at last.

2 Modeling

Assume that one unit cell of the periodic structure portrayed in Fig. 1 is meshed employing three-dimensional FEs, considering the acoustic fluid and solid behaviors. Their corresponding mass and stiffness matrices are then extracted from conventional FE software, and by considering fluid and structural damping effects, one can write [17]:

$$\hat{\mathbf{M}}\ddot{\hat{\mathbf{q}}}+\hat{\mathbf{C}}\dot{\hat{\mathbf{q}}}+\hat{\mathbf{K}}\hat{\mathbf{q}}=\hat{\mathbf{F}}\,, \tag{1}$$

where $\dot{(\,)}$ represents derivatives with respect to time and:

$$\hat{\mathbf{M}} = \begin{bmatrix} \mathbf{M}_{\mathrm{S}} & \mathbf{0} \\ \rho\mathbf{R}^{\mathrm{T}} & \mathbf{M}_{\mathrm{A}} \end{bmatrix},\ \hat{\mathbf{C}} = \begin{bmatrix} \mathbf{C}_{\mathrm{S}} & \mathbf{0} \\ \mathbf{0} & \mathbf{C}_{\mathrm{A}} \end{bmatrix},\ \hat{\mathbf{K}} = \begin{bmatrix} \mathbf{K}_{\mathrm{S}} & -\mathbf{R} \\ \mathbf{0} & \mathbf{K}_{\mathrm{A}} \end{bmatrix},\ \hat{\mathbf{q}} = \begin{Bmatrix} \hat{\mathbf{U}} \\ \hat{\mathbf{p}} \end{Bmatrix},\ \hat{\mathbf{F}} = \begin{Bmatrix} \hat{\mathbf{F}}_{\mathrm{S}} \\ \hat{\mathbf{F}}_{\mathrm{A}} \end{Bmatrix}. \quad (2)$$

In the two previous equations, $\mathbf{M}_j$, $\mathbf{C}_j$, $\mathbf{K}_j$ $\left(j \in \{\mathrm{S},\mathrm{A}\}\right)$ stand for mass, viscous damping and stiffness matrices of structure (S) and acoustic-fluid (A) parts; $\mathbf{R}$ stands for the fluid-structure coupling matrix; $\ddot{\hat{\mathbf{U}}}$, $\dot{\hat{\mathbf{U}}}$, $\hat{\mathbf{U}}$, and $\hat{\mathbf{F}}_{\mathrm{A}}$ are generalized acceleration, velocity, displacement, and load vectors of the structure domain; $\ddot{\hat{\mathbf{p}}}$, $\dot{\hat{\mathbf{p}}}$, $\hat{\mathbf{p}}$, and $\hat{\mathbf{F}}_{\mathrm{S}}$ are generalized acceleration, velocity, displacement, and load vectors related to the internal fluid ($\hat{\mathbf{p}}$ referring to pressure); ρ is the fluid density; and $(\,)^{\mathrm{T}}$ is the transpose operator.

As discussed in Section 1, the use of WFEM may become challenging in certain conditions where a high number of internal DoFs is found. To overcome this computational trouble, DoFs that are not located in the unit cell's left (L) and right (R) interfaces, namely internal (I), can be reduced by employing the CB model order reduction method. The procedure, basically, consists of establishing the following transformation matrix:

$$\boldsymbol{\alpha} = \begin{bmatrix} \mathbf{I} & \mathbf{0} \\ \boldsymbol{\Phi}_{\mathrm{C}} & \boldsymbol{\Phi}_{\mathrm{N}} \end{bmatrix}, \quad (3)$$

where $\mathbf{I}$ is an identity matrix, $\boldsymbol{\Phi}_{\mathrm{C}} = \hat{\mathbf{K}}_{\mathrm{II}}^{-1}\hat{\mathbf{K}}_{\mathrm{IB}}$ (B accounts for boundary DoFs comprising those located in both left and right interfaces), and $\boldsymbol{\Phi}_{\mathrm{N}}$ is a matrix of eigenvectors obtained from an eigenproblem that represents the dynamics of the considered unit cell with boundary DoFs constrained [19]. Since $\hat{\mathbf{q}} = \boldsymbol{\alpha}\mathbf{q}$, the reduced set of equations of motion can be written as:

$$\mathbf{M}\ddot{\mathbf{q}} + \mathbf{C}\dot{\mathbf{q}} + \mathbf{K}\mathbf{q} = \mathbf{F}\,, \quad (4)$$

with $\mathbf{M} = \boldsymbol{\alpha}^{\mathrm{T}}\hat{\mathbf{M}}\boldsymbol{\alpha}$, $\mathbf{C} = \boldsymbol{\alpha}^{\mathrm{T}}\hat{\mathbf{C}}\boldsymbol{\alpha}$, $\mathbf{K} = \boldsymbol{\alpha}^{\mathrm{T}}\hat{\mathbf{K}}\boldsymbol{\alpha}$, and $\mathbf{F} = \boldsymbol{\alpha}^{\mathrm{T}}\hat{\mathbf{F}}$. It is worth noting that a modified version of the previously mentioned model reduction methodology might be employed to address structural systems interacting with enclosed acoustic fluids, as discussed elsewhere [20].

The reduced coupled fluid-structure equations seen before in Eq. (4) can be rewritten in the frequency domain as $\mathbf{D}\mathbf{q} = \mathbf{F}$, where $\mathbf{D} = -\omega^2\mathbf{M} + \mathrm{i}\omega\mathbf{C} + \mathbf{K}$, i is the imaginary unit, and ω is the circular frequency. Following the basic procedure of the WFEM, the reduced DoFs and load vectors can be explicitly organized with respect to their position in the unit cell:

$$\begin{bmatrix} \mathbf{D}_{\mathrm{LL}} & \mathbf{D}_{\mathrm{LR}} & \mathbf{D}_{\mathrm{LI}} \\ \mathbf{D}_{\mathrm{RL}} & \mathbf{D}_{\mathrm{RR}} & \mathbf{D}_{\mathrm{RI}} \\ \mathbf{D}_{\mathrm{IL}} & \mathbf{D}_{\mathrm{IR}} & \mathbf{D}_{\mathrm{II}} \end{bmatrix} \begin{Bmatrix} \mathbf{q}_{\mathrm{L}} \\ \mathbf{q}_{\mathrm{R}} \\ \mathbf{q}_{\mathrm{I}} \end{Bmatrix} = \begin{Bmatrix} \mathbf{F}_{\mathrm{L}} \\ \mathbf{F}_{\mathrm{R}} \\ \mathbf{F}_{\mathrm{I}} \end{Bmatrix}, \tag{5}$$

which may be used to obtain an expression that relates DoFs and load vectors of the left interface between two adjacent unit cells of a periodic structure, the $(n+1)$ and (n), i.e., $\mathbf{u}_{\mathrm{L}}^{(n+1)} = \mathbf{S}\mathbf{u}_{\mathrm{L}}^{(n)} + \mathbf{b}^{(n)}$. This recurrence relation incorporates the unit cell state vector $\mathbf{u}_{\mathrm{L}} = \{\mathbf{q}_{\mathrm{L}}^{\mathrm{T}}\ \mathbf{F}_{\mathrm{L}}^{\mathrm{T}}\}^{\mathrm{T}}$, a transfer matrix $\mathbf{S}$, and a forcing vector related to external loads $\mathbf{b}$ [21].

Bloch-Floquet theorem can be resorted to, so that the recurrence relation stated before leads to $(\mathbf{S} - \mu_j \mathbf{I})\boldsymbol{\varphi}_j = \mathbf{0}$. Here, μ_j and $\boldsymbol{\varphi}_j$ ($j \in \{1, ..., 2 \times n_b\}$), being n_b the number of DoFs in the left (or right) interface of the unit cell, are eigen-solutions (wave-modes) of the transfer matrix eigenproblem that physically represent the propagation constant and wave shapes, respectively. Wavenumbers can be computed from propagation constants as $k_j = (\ln \mu_j)/(-\mathrm{i}\Delta)$, where Δ is the length of the unit cell along the direction of wave propagation – assumed to be in the X-direction, cf. Fig. 1. As discussed by Waki et al. [22] and Mencik [23], the standard eigenvalue problem described earlier may be prone to numerical issues due to ill-conditioning problems. Thus, to alleviate potential computational challenges, one can resort to the alternative formulation $(\mathbf{N}\mathbf{J}\mathbf{L}^{\mathrm{T}} + \mathbf{L}\mathbf{J}\mathbf{N}^{\mathrm{T}} - \lambda_j \mathbf{L}\mathbf{J}\mathbf{L}^{\mathrm{T}})\mathbf{z}_j = \mathbf{0}$ [24], where λ_j and $\mathbf{z}_j$ are eigen-solutions of Zhong's eigenvalue problem – expressions for $\mathbf{N}$, $\mathbf{J}$, and $\mathbf{L}$ can be found in [25]. The set of wave-modes associated with the transfer matrix eigenvalue problem $(\mu_j, \boldsymbol{\varphi}_j)$ can be retrieved from λ_j and $\mathbf{z}_j$, following the procedure outlined in [25].

Wave-modes computed as discussed previously can be grouped with respect to the direction of wave propagation, i.e., in positive- $(\mu_j, \boldsymbol{\varphi}_j)$ and negative-going waves $(\mu_j^*, \boldsymbol{\varphi}_j^*)$ as follows [26, 27]:

$$\begin{aligned} \boldsymbol{\mu} &= \mathrm{diag}(\mu_1, \ldots, \mu_{n_b}), & \boldsymbol{\mu}^* &= \mathrm{diag}(\mu_1^*, \ldots, \mu_{n_b}^*), \\ \boldsymbol{\Phi} &= [\boldsymbol{\varphi}_1 \ldots \boldsymbol{\varphi}_{n_b}] = \begin{bmatrix} \boldsymbol{\Phi}_q \\ \boldsymbol{\Phi}_F \end{bmatrix}, & \boldsymbol{\Phi}^* &= [\boldsymbol{\varphi}_1^* \ldots \boldsymbol{\varphi}_{n_b}^*] = \begin{bmatrix} \boldsymbol{\Phi}_q^* \\ \boldsymbol{\Phi}_F^* \end{bmatrix}, \end{aligned} \tag{6}$$

with subscripts q and F used to denote partitions of the wave shapes related to DoFs and loads, respectively. To develop expressions presented afterward, one highlights that eigenvectors must be normalized as described in [23]. In addition, since the wave-modes are computed for each desired frequency independently, some frequency tracking procedure might be used to better visualize dispersion curves, i.e., the relation between wavenumbers and frequency. Given a pair of wave-modes related to eigenvalues μ_a and μ_a^*, with $\mu_a = 1/\mu_a^*$, the wave-mode corresponding to μ_a at the consecutive frequency $\omega + \delta_\omega$ is chosen so that [28]:

$$\left|\frac{\boldsymbol{\varphi}_a^{*\mathrm{T}}(\omega)}{\left\|\boldsymbol{\varphi}_a^{*}(\omega)\right\|}\mathbf{J}\frac{\boldsymbol{\varphi}_a(\omega+\delta_\omega)}{\left\|\boldsymbol{\varphi}_a(\omega+\delta_\omega)\right\|}\right| = \max_{b\in\{1,\ldots,n_b\}}\left\{\left|\frac{\boldsymbol{\varphi}_a^{*\mathrm{T}}(\omega)}{\left\|\boldsymbol{\varphi}_a^{*}(\omega)\right\|}\mathbf{J}\frac{\boldsymbol{\varphi}_b(\omega+\delta_\omega)}{\left\|\boldsymbol{\varphi}_b(\omega+\delta_\omega)\right\|}\right|\right\}, \tag{7}$$

where $\|\quad\|$ denotes the norm of a vector and $|\quad|$ denotes the absolute value of a scalar.

Lastly, the forced response of a finite structure with N unit cells can be calculated using the following expressions [21]:

$$\mathbf{q}_{\mathrm{L}}^{(n)} = \boldsymbol{\Phi}_q\boldsymbol{\mu}^{n-1}\mathbf{Q} + \boldsymbol{\Phi}_q^{*}\boldsymbol{\mu}^{N+1-n}\mathbf{Q}^{*} + \boldsymbol{\Phi}_q\sum_{k=1}^{n-1}\boldsymbol{\mu}^{n-k-1}\mathbf{Q}_B^{(k)} - \boldsymbol{\Phi}_q^{*}\sum_{k=n}^{N}\boldsymbol{\mu}^{k+1-n}\mathbf{Q}_B^{*(k)}, \tag{8}$$

$$-\mathbf{F}_{\mathrm{L}}^{(n)} = \boldsymbol{\Phi}_F\boldsymbol{\mu}^{n-1}\mathbf{Q} + \boldsymbol{\Phi}_F^{*}\boldsymbol{\mu}^{N+1-n}\mathbf{Q}^{*} + \boldsymbol{\Phi}_F\sum_{k=1}^{n-1}\boldsymbol{\mu}^{n-k-1}\mathbf{Q}_B^{(k)} - \boldsymbol{\Phi}_F^{*}\sum_{k=n}^{N}\boldsymbol{\mu}^{k+1-n}\mathbf{Q}_B^{*(k)}, \tag{9}$$

being $\mathbf{Q}_B^{(k)}$ and $\mathbf{Q}_B^{*(k)}$ amplitudes of externally applied loads in the wave-basis space; $\mathbf{Q}\equiv\mathbf{Q}^{(1)}$ and $\mathbf{Q}^{*}\equiv\mathbf{Q}^{*(N+1)}$ wave-mode amplitudes for the first (1) and $(N+1)$ unit cells. Equations (8) and (9) can be used to enforce boundary conditions and establish a linear system of equations for the unknowns $\mathbf{Q}$ and $\mathbf{Q}^{*}$. Solving this system enables the determination of any response of the periodic structure. For the sake of clarity, in our case, aiming to simulate a free-free condition, $\mathbf{F}_{\mathrm{L}}^{(1)}=\mathbf{0}$ and $\mathbf{F}_{\mathrm{L}}^{(N+1)}=\mathbf{0}$ must be written, so that one obtains [29]:

$$\begin{bmatrix}\mathbf{I} & \boldsymbol{\Phi}_F^{-1}\boldsymbol{\Phi}_F^{*}\boldsymbol{\mu}^{N}\\ \boldsymbol{\Phi}_F^{*-1}\boldsymbol{\Phi}_F\boldsymbol{\mu}^{N} & \mathbf{I}\end{bmatrix}\begin{Bmatrix}\mathbf{Q}\\ \mathbf{Q}^{*}\end{Bmatrix} = \begin{Bmatrix}\boldsymbol{\Phi}_F^{-1}\boldsymbol{\Phi}_F^{*}\sum_{k=1}^{N}\boldsymbol{\mu}^{k}\mathbf{Q}_B^{*(k)}\\ -\boldsymbol{\Phi}_F^{*-1}\boldsymbol{\Phi}_F\sum_{k=1}^{N}\boldsymbol{\mu}^{N-k}\mathbf{Q}_B^{(k)}\end{Bmatrix}. \tag{10}$$

3 Experimental and numerical results

In the following, experimental and numerical results will be presented, as well as the experimental procedures we employed. Section 3.1 first presents manufacturing considerations and details about the FE model of a unit cell of the periodic structure without confined fluid. Related numerical and experimental findings are compared

in Section 3.2, where FRFs of the fluid-filled metastructure are made available to assess its wave propagation characteristics.

3.1 Manufacturing considerations and finite element model

The three-dimensional systems examined in this study comprise rectangular parallelepiped unit cells with external dimensions equal to 60 mm × 10 mm × 30 mm ($\Delta = 60$ mm), containing a perfectly centered internal rectangular parallelepiped void, measuring 53.6 mm × 6 mm × 23.6 mm. The numerical and experimental analyses presented here initially focus on the dynamic behavior of the periodic metastructure illustrated in Fig. 1 without internal fluid. A three-dimensional model of the system was created using computer-aided engineering (CAD) software and was subsequently made in separate parts using additive manufacturing, as depicted in Fig. 2a. Due to manufacturing limitations, the base of the periodic structure was printed first, resulting in the configuration depicted in Fig. 2b. Subsequently, the cap was produced with a nominal thickness of 2 mm, leading to the geometry displayed in Fig. 2c. Finally, the cap was bonded to the base of the metastructure using cyanoacrylate superglue, completing the system shown in Fig. 2d.

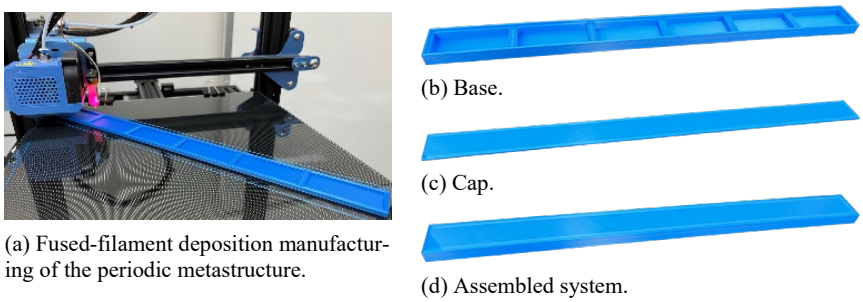

(a) Fused-filament deposition manufacturing of the periodic metastructure.

(b) Base.

(c) Cap.

(d) Assembled system.

Fig. 2 Manufacture details of the periodic metastructure with voids (without fluid).

To conduct numerical investigations on the previously depicted system, the terms appearing in the equations of motion for the unit cell, as shown in Eq. (1), are reduced to $\hat{\mathbf{M}} = \mathbf{M}_S$, $\hat{\mathbf{C}} = \mathbf{C}_S$, $\hat{\mathbf{K}} = \mathbf{K}_S$, $\hat{\mathbf{q}} = \hat{\mathbf{U}}$, and $\hat{\mathbf{F}} = \hat{\mathbf{F}}_S$. The mass and stiffness matrices mentioned earlier are obtained from conventional FE software employing linear interpolation functions and material with linear behavior and utilizing the FE mesh illustrated in Fig. 3. Specifically, 4-noded tetrahedral elements with three DoFs per node are used, i.e., encompassing translations in the *X*, *Y*, and *Z*-directions cf. Fig. 1. Furthermore, the modelling of the unit cell incorporates a total of 75242 FEs, which satisfactorily ensures the model convergence up to the maximum analyzed frequency of 5000 Hz. The structure is made of polylactic acid (PLA), for which one assumed an elastic modulus of 2.24 GPa, density of 1052.6 kg m^{-3}, and Poisson's ratio of 0.3. Viscous damping was not considered in this study ($\hat{\mathbf{C}} = \mathbf{0}$).

However, dissipation effects in the system's forced responses were accounted for through hysteretic damping, i.e., using $\hat{\mathbf{K}} = (1+\mathrm{i}\eta)\mathbf{K}_S$, with η being the structural damping coefficient, set to 0.02. Moreover, a complete wave basis comprising 714 left- and right-going wave-modes (i.e., $n_b = 357$) was employed to characterize the dynamics of the unit cell under investigation. This choice was based on the demonstrated relevance of some evanescent wave-modes in the dynamics of the examined system, during numerical validations of the wave-based approach against FE analyses. These evanescent wave-modes may be reflected by the internal boundaries near the excitation location and, therefore, should not be neglected when computing responses for a finite system with relatively small length. It is noteworthy that even when considering the complete wave basis to describe the behavior of the metastructure, one solves a significantly smaller linear system of equations compared to traditional FEM.

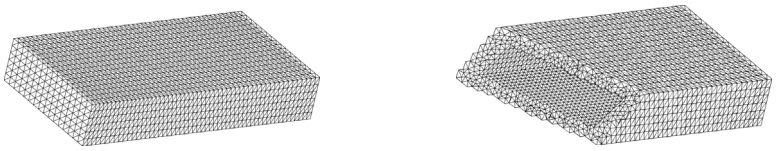

(a) Unit cell mesh. (b) Cut revealing the internal void and wall mesh.

Fig. 3 Finite element mesh used to model the unit cells of the periodic metastructure shown in Fig. 1, without internal fluid, using the Wave-based Finite Element Method.

3.2 Comparison between numerical and experimental results

First and foremost, the theory briefly discussed in Section 2 can be employed to calculate the dispersion curves for an infinite and undamped $(\eta = 0)$ metastructure consisting of unit cells without internal fluid. Since the analyzed system does not exhibit any non-reciprocal properties in terms of wave propagation characteristics, the dispersion curves show symmetry with respect to the frequency axis. Therefore, Fig. 4 displays only the positive values of $\mathrm{Re}\{k_j\}$ and the corresponding negative values of $\mathrm{Im}\{k_j\}$ to visualize the dispersion branches. In Fig. 4, only the first four pairs of wavenumbers, related to wave-modes that propagate (or spatially decay) to left and right directions, were depicted instead of all those 714 computed for convenience. It is important to note that these wave-modes are related to propagating and evanescent modes and may be associated with longitudinal, bending, torsional, and shear wave types. The focus here is on the wave-modes that most influence the longitudinal and bending dynamics in the *X*- and *Y*-directions, respectively, cf. Fig. 1, whose corresponding dispersion branches are duly identified in Fig. 4.

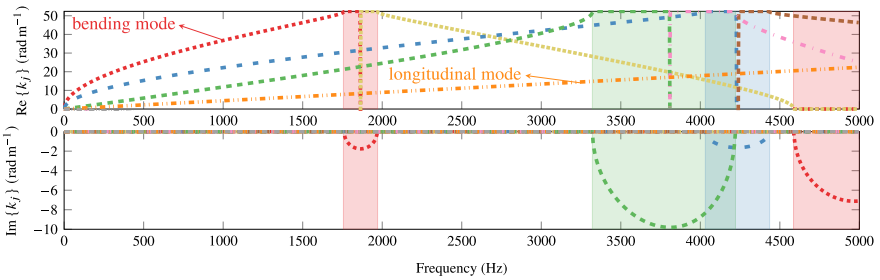

Fig. 4 Dispersion curves, positive values of $\mathrm{Re}\{k_j\}$ and negative values of $\mathrm{Im}\{k_j\}$, and bandgaps frequency ranges $(\mathrm{Im}\{k_j\} \neq 0)$ computed for the undamped $(\eta = 0)$ unit cell of the periodic structure shown in Fig. 1, without confined fluid. The correspondence between wavenumbers depicted in $\mathrm{Re}\{k_j\}$ and $\mathrm{Im}\{k_j\}$ is illustrated by the dispersion curves with matching colors and line styles.

In addition to the dispersion curves shown in Fig. 4, bandgap frequency ranges are also illustrated, corresponding to those frequency ranges for which $\mathrm{Im}\{k_j\} \neq 0$. To aid comprehension, these frequency bands are highlighted using shaded areas in colors that correspond to those used to plot the negative values of $\mathrm{Im}\{k_j\}$. Furthermore, to enhance clarity, a summary of these bandgap frequency ranges is provided in Table 1. Thus, based on the curves shown in Fig. 4 and the results provided in Table 1, it is evident that the investigated system exhibits four distinct forbidden zones up to 5 kHz.

Table 1 A summary of the bandgap frequency ranges $(\mathrm{Im}\{k_j\} \neq 0)$ seen in Fig.4, computed for an undamped $(\eta = 0)$ and infinite metastructure made with the unit cell shown in Fig.1, without internal fluid.

Line styles used in Fig. 4	Bandgap frequency ranges (Hz)
and	(1756 – 1971), (4586 – 5000)
and	(3321 – 4221)
and	(4031 – 4436)

To validate the previously observed numerical predictions regarding the bandgap frequency ranges calculated for an infinite system, the wave propagation behavior of a finite system with $N = 6$ unit cells is considered, cf. Fig. 2d. Accelerance-type FRFs are measured in the longitudinal and transversal directions (X- and Y-directions, respectively), with the experimental setups for these measurements shown in Figs. 5a and 5b. For the investigation of the longitudinal behavior of the periodic system, the experimental scheme shown in Fig. 5a was utilized. An accelerometer PCB 352C22 was positioned at the leftmost face of the structure, while an impulsive force was applied at its right end. Both the input and output positions were located precisely at the center of the relevant cross-sections. On the other hand, the bending behavior of the system was examined using the experimental setup depicted in Fig. 5b. In this case, the structure was spatially reoriented to minimize the influence of nylon strings on the free vibration of the system. For this scenario, the accelerometer was again placed at the midpoint of the leftmost boundary, but in the XZ-plane. The

hammer excitation force was directed along the Y direction, being applied at the rightmost edge of the structure. Comparisons between numerical and experimental findings are presented in Figs. 5c and 5d for longitudinal and bending dynamics, respectively. It is important to note that the numerical curves were computed using the theory discussed in Section 2, specifically by applying Eq. (8).

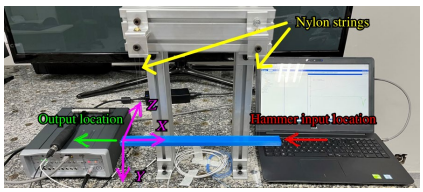

(a) Setup used to investigate the longitudinal behavior of the periodic metastructure.

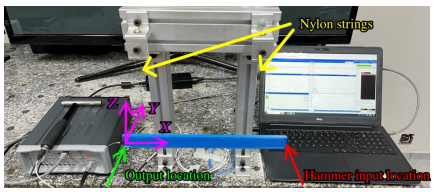

(b) Setup used to investigate the bending behavior of the periodic metastructure.

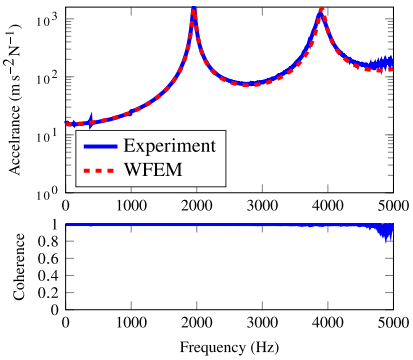

(c) A comparison between numerical and experimental FRFs corresponding to the input and output locations seen in Fig. 5a.

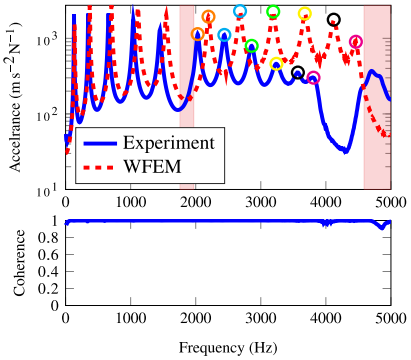

(d) A comparison between numerical and experimental FRFs corresponding to the input and output locations seen in Fig. 5b.

Fig. 5 Experimental setups and comparisons between numerical and measured FRFs used to investigate the longitudinal and bending behavior of the periodic metastructure portrayed in Figs. 1 and 2, without internal fluid.

As one may notice from Fig. 5c, the numerical prediction matches well the experimental result obtained through the hammer test across the entire frequency range considered. Both resonance frequencies related to the longitudinal motion of the system are accurately predicted, corresponding to approximately 1960 Hz and 3890 Hz. In addition, the experimental FRF also exhibit strong agreement with the wave-based model far from the resonance conditions. Moreover, the numerical predictions regarding the wave propagation behavior of longitudinal modes, provided by the Bloch-Floquet theorem, as depicted in Fig. 4, are further supported by these FRFs. This means that the finite system did not experience attenuation zones in the considered frequency range regarding the propagation of longitudinal waves, since the dispersion curve seen in Fig. 4, related to this kind of motion, is purely real. Lastly, the coherence function depicted in Fig. 5c confirms the good quality of the experimental data, indicating a well-conducted experiment.

On the other hand, a comparison between numerical and experimental results depicted in Fig. 5d reveals that the wave-based model does not accurately describe the bending motion of the periodic structure without fluid, even with its longitudinal dynamics being properly predicted, as shown by Fig. 5c. In fact, the natural frequencies computed using the WFEM are larger than those identified from experimental data, indicating that the model exhibits a stiffer behavior. However, it is noteworthy that the number of resonance peaks observed in the numerical results perfectly matches those related to experiments – cf. indicated in Fig. 5d. Furthermore, the predictions derived from the Bloch-Floquet theorem regarding the attenuation zone of bending modes are confirmed by the numerical FRF shown in Fig. 5d. This shows that the finite system exhibits two forbidden zones up to 5 kHz, as illustrated by the shaded areas in red. These attenuation zones are close to the steep valleys related to the blue curve, potentially corresponding to the actual attenuation zones of the tested finite system. Nevertheless, the forbidden zones identified through experiments are slightly shifted to the left, as previously discussed for the natural frequencies. This frequency shift can be attributed mainly to our assumption of a linear, isotropic constitutive relationship for the material, which does not fully reflect the system's actual behavior, as well as uncertainties in the PLA material properties assumed by us. For instance, the material is known to exhibit viscoelastic behavior [30], and the additive manufacturing process we employed favors the resulting media to possess orthotropic symmetry [31]. Notwithstanding, we chose to consider a linear model for our analysis, which still yields a fair match with the experimental data. It is also worth mentioning that the coherence function associated with the bending-type motion test is good, similarly to the results shown in Fig. 5c, also indicating well-conducted experiments.

To experimentally assess the dynamic behavior of the system depicted in Fig. 2d, with unit cells completely filled with water, new experiments were conducted. Firstly, another periodic structure was manufactured, following the procedures described in Section 3.1. The surfaces of the six-cell periodic system that could potentially come into contact with water were sealed using varnish, to waterproof the prototype model. Subsequently, the internal cavities were filled with fluid, and the cap was glued to the superior part of the base of the periodic structure. By adopting the same experimental setups discussed earlier and shown in Figs. 5a and 5b, longitudinal and bending accelerance-type FRFs were measured employing hammer tests for the water-filled system. Associated results are provided in Fig. 6. The same figure also includes the experimental FRFs obtained for the metastructure without fluid, previously shown in Figs. 5c and 5d, for convenience and ease of comparison.

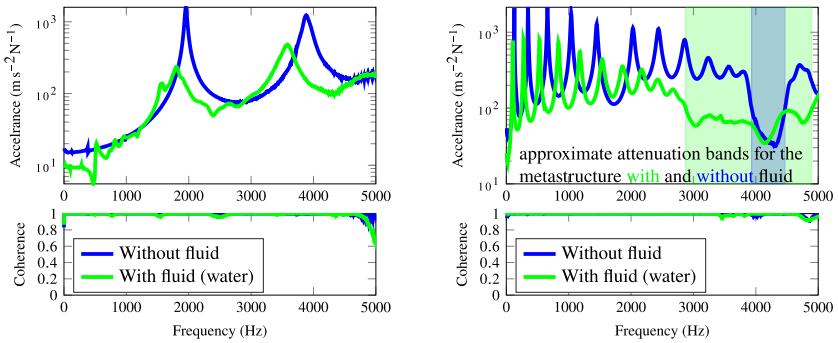

(a) Longitudinal FRFs corresponding to the input and output locations seen in Fig. 5c.

(b) Bending FRFs corresponding to the input and output locations seen in Fig. 5d.

Fig. 6 Comparisons between experimental FRFs measured for the periodic system portrayed in Fig. 1, with and without internal fluid, to investigate its longitudinal and bending dynamic behavior.

First, Figs. 6a and 6b show that most resonance peaks exist in both conditions when the system is without or completely filled with fluid. This observation was previously made by Spadoni et al. [10], where these modes were referred to as persistent modes. In addition, a comparison between the blue and green curves depicted in Figs. 6a and 6b reveals that the internal fluid significantly contributes to damping effects in the finite periodic system. This is evident from the noticeable attenuation of amplitudes at the resonance frequencies associated to the green curve in Fig. 6b. Turning attention to Fig. 6a, additional resonances emerge when the periodic system is filled with fluid, which may be associated with acoustic modes. Confirmation of this observation would require an examination of the system's deformed shapes at the corresponding frequencies. Additionally, the results shown in Fig. 6b, related to bending dynamics, demonstrate that the region corresponding to the second experimental attenuation zone is significantly wider when the cavities are completely filled with water, in comparison to the condition without internal fluid, as illustrated schematically using shading. This finding suggests a novel way to broaden attenuation zones in metamaterials by leveraging the dynamic behavior of fluid-filled cells. Moreover, this realization confirms the outstanding performance of fluid-filled metamaterials in vibroacoustics in terms of attenuating elasto-acoustic waves.

Concluding remarks

This study investigated the dynamic behavior of periodic structures with internal cavities completely filled with water and in the absence of it. We reviewed a general formulation based on the WFEM to analyze wave propagation phenomena in fluid-filled systems. Utilizing this wave-based modeling approach, simulations were conducted to investigate the dynamics of the periodic system without internal fluid.

Additionally, dispersion curves were computed using the Bloch-Floquet theorem for the unit cell lacking fluid, providing insights into the wave propagation characteristics through the considered finite system. Experimental tests were conducted on a finite metastructure comprising six unit cells without fluid, and measured accelerance FRFs exhibited good agreement with predictions provided by the wave-based model. Furthermore, attenuation zones predicted by the Bloch-Floquet theorem were confirmed in both numerical and experimental accelerance responses. Moreover, the dynamic behavior of the metastructure made with fluid-filled unit cells was experimentally assessed through hammer tests. A comparison between the experimental FRFs of the regarded periodic structure without and with internal fluid revealed that the frequency range near the second attenuation band observed in the former case can be significantly enlarged in the presence of fluid within the unit cells' cavities. This indicates the potential of using such metamaterials as a novel passive vibration absorber mechanism in various vibroacoustic engineering applications.

Acknowledgments V. M. S. Santos acknowledges his current doctorate scholarship grant #23/11207-7 from the São Paulo Research Foundation (FAPESP), and the Brazilian Coordination for the Improvement of Higher Education Personnel (CAPES). V. M. S. Santos and T. P. Sales are grateful to the FAPESP for its support to the thematic grant #18/15894-0, related to the "Periodic structure design and optimization for enhanced vibroacoustic performance: ENVIBRO" research project. M. Ouisse acknowledges the graduate school EIPHI (project ANR-17-EURE-0002).

References

1. Pal, R.K., Ruzzene, M.: Edge waves in plates with resonators: an elastic analogue of the quantum valley Hall effect. New J. Phys. 19, 025001 (2017). https://doi.org/10.1088/1367-2630/aa56a2
2. Wu, T.-C., Wu, T.-T., Hsu, J.-C.: Waveguiding and frequency selection of Lamb waves in a plate with a periodic stubbed surface. Phys. Rev. B. 79, (2009). https://doi.org/10.1103/physrevb.79.104306
3. Ning, L., Wang, Y.-Z., Wang, Y.-S.: Active control cloak of the elastic wave metamaterial. Int. J. Solids Struct. 202, 126–135 (2020). https://doi.org/10.1016/j.ijsolstr.2020.06.009
4. Wang, H., Xu, Y., Genevet, P., Jiang, J.-H., Chen, H.: Broadband mode conversion via gradient index metamaterials. Sci. Rep. 6, (2016). https://doi.org/10.1038/srep24529

5. Gao, N., Zhang, Z., Deng, J., Guo, X., Cheng, B., Hou, H.: Acoustic Metamaterials for Noise Reduction: A Review. Adv. Mater. Technol. 7, 2100698 (2022). https://doi.org/10.1002/admt.202100698
6. Miranda, E.J.P., Nobrega, E.D., Ferreira, A.H.R., Santos, J.M.C.D.: Flexural wave band gaps in a multi-resonator elastic metamaterial plate using Kirchhoff-Love theory. Mech. Syst. Signal Pr. 116, 480–504 (2019). https://doi.org/10.1016/j.ymssp.2018.06.059
7. Nobrega, E.D., Gautier, F., Pelat, A., Santos, J.M.C.D.: Vibration band gaps for elastic metamaterial rods using wave finite element method. Mech. Syst. Signal Pr. 79, 192–202 (2016). https://doi.org/10.1016/j.ymssp.2016.02.059
8. Mizukami, K., Funaba, K., Ogi, K.: Design and three-dimensional printing of carbon-fiber-composite elastic metamaterials with inertial amplification mechanisms. J. Sound Vib. 513, 116412 (2021). https://doi.org/10.1016/j.jsv.2021.116412
9. Jamshidiat, H., SenGupta, G.: Dynamics of periodic structures interacting with an enclosed fluid medium. J. Sound Vib. 148, 103–115 (1991). https://doi.org/10.1016/0022-460x(91)90822-2
10. Spadoni, A., Höhler, R., Cohen-Addad, S., Dorodnitsyn, V.: Closed-cell crystalline foams: Self-assembling, resonant metamaterials. J. Acoust. Soc. Am. 135, 1692–1699 (2014). https://doi.org/10.1121/1.4867375
11. Dorodnitsyn, V., Damme, B.V.: Two-dimensional fluid-filled closed-cell cellular solid as an acoustic metamaterial with negative index. Phys. Rev. B. 93, 134302 (2016). https://doi.org/10.1103/physrevb.93.134302
12. Mirsky, I., Herrmann, G.: Nonaxially Symmetric Motions of Cylindrical Shells. J. Acoust. Soc. Am. 29, 1116–1123 (1957). https://doi.org/10.1121/1.1908716
13. McNiven, H.D., Sackman, J.L., Shah, A.H.: Axially Symmetric Waves in Hollow, Elastic Rods. Part II. J. Acoust. Soc. Am. 40, 1073–1076 (1966). https://doi.org/10.1121/1.1910190
14. Bao, X.L., Überall, H., Raju, P.K., Ahyi, A.C., Bjo/rno, I.K., Bjo/rno, L.: Dispersion of axially symmetric waves in fluid-filled cylindrical shells. J. Acoust. Soc. Am. 107, 2847–2848 (2000). https://doi.org/10.1121/1.429206
15. Kumar, R., Stephens, R.W.B.: Dispersion of flexural waves in circular cylindrical shells. Proc. R. Soc. Lond. A. 329, 283–297 (1972). https://doi.org/10.1098/rspa.1972.0114
16. Fuller, C.R., Fahy, F.J.: Characteristics of wave propagation and energy distributions in cylindrical elastic shells filled with fluid. J. Sound Vib. 81, 501–518 (1982). https://doi.org/10.1016/0022-460x(82)90293-0
17. Mencik, J.-M., Ichchou, M.N.: Wave finite elements in guided elastodynamics with internal fluid. Int. J. Solids Struct. 44, 2148–2167 (2007). https://doi.org/10.1016/j.ijsolstr.2006.06.048
18. Droz, C., Lainé, J.-P., Ichchou, M.N., Inquiété, G.: A reduced formulation for the free-wave propagation analysis in composite structures. Compos. Struct. 113, 134–144 (2014). https://doi.org/10.1016/j.compstruct.2014.03.017
19. Mencik, J.-M.: A wave finite element approach for the analysis of periodic structures with cyclic symmetry in dynamic substructuring. J. Sound Vib. 431, 441–457 (2018). https://doi.org/10.1016/j.jsv.2018.05.027

20. Maess, M., Gaul, L.: Substructuring and model reduction of pipe components interacting with acoustic fluids. Mech. Syst. Signal Pr. 20, 45–64 (2006). https://doi.org/10.1016/j.ymssp.2005.02.008
21. Hoang, T., Duhamel, D., Foret, G.: Wave finite element method for waveguides and periodic structures subjected to arbitrary loads. Finite Elem. Anal. Des. 179, 103437 (2020). https://doi.org/10.1016/j.finel.2020.103437
22. Waki, Y., Mace, B.R., Brennan, M.J.: Numerical issues concerning the wave and finite element method for free and forced vibrations of waveguides. J. Sound Vib. 327, 92–108 (2009). https://doi.org/10.1016/j.jsv.2009.06.005
23. Mencik, J.-M.: New advances in the forced response computation of periodic structures using the wave finite element (WFE) method. Comput. Mech. 54, 789–801 (2014). https://doi.org/10.1007/s00466-014-1033-1
24. Zhong, W.X., Williams, F.W.: On the direct solution of wave propagation for repetitive structures. J. Sound Vib. 181, 485–501 (1995). https://doi.org/10.1006/jsvi.1995.0153
25. Mencik, J.-M., Duhamel, D.: A wave-based model reduction technique for the description of the dynamic behavior of periodic structures involving arbitrary-shaped substructures and large-sized finite element models. Finite Elem. Anal. Des. 101, 1–14 (2015). https://doi.org/10.1016/j.finel.2015.03.003
26. Duhamel, D., Mace, B.R., Brennan, M.J.: Finite element analysis of the vibrations of waveguides and periodic structures. J. Sound Vib. 294, 205–220 (2006). https://doi.org/10.1016/j.jsv.2005.11.014
27. Waki, Y., Mace, B.R., Brennan, M.J.: Free and forced vibrations of a tyre using a wave/finite element approach. J. Sound Vib. 323, 737–756 (2009). https://doi.org/10.1016/j.jsv.2009.01.006
28. Mencik, J.-M.: On the low- and mid-frequency forced response of elastic structures using wave finite elements with one-dimensional propagation. Comput. Struct. 88, 674–689 (2010). https://doi.org/10.1016/j.compstruc.2010.02.006
29. Santos, V.M.S.: Numerical Investigation of Wave Propagation in Beams Coupled to Metastructures Combining Spectral and Wave-Finite Element Methods, (2022)
30. Müller, M., Šleger, V., Kolář, V., Hromasová, M., Piš, D., Mishra, R.K.: Low-Cycle Fatigue Behavior of 3D-Printed PLA Reinforced with Natural Filler. Polymers. 14, 1301 (2022). https://doi.org/10.3390/polym14071301
31. Torre, R., Brischetto, S.: Experimental characterization and finite element validation of orthotropic 3D-printed polymeric parts. Int. J. Mech. Sci. 219, 107095 (2022). https://doi.org/10.1016/j.ijmecsci.2022.107095